Journal of Power Sources 253 (2014) 349–359

Contents lists available at ScienceDirect

Journal of Power Sources

journal homepage: www.elsevier.com/locate/jpowsour

Composite cathode based on doped vanadate enhanced with loaded metal nanoparticles for steam electrolysis

Yuanxin Li [a], Guojian Wu [a], Cong Ruan [a], Qi Zhou [a], Yan Wang [a], Winston Doherty [c], Kui Xie [a,b,*], Yucheng Wu [a,b,*]

[a] Department of Energy Materials, School of Materials Science and Engineering, Hefei University of Technology, No. 193 Tunxi Road, Hefei, Anhui 230009, China
[b] Key Laboratory of Advanced Functional Materials and Devices of Anhui Province, Hefei University of Technology, No. 193 Tunxi Road, Hefei, Anhui 230009, China
[c] School of Applied Sciences and Engineering, Gippsland Campus, Monash University, Churchill 3842, Victoria, Australia

HIGHLIGHTS

- The synergetic effect was achieved in the nanometal-loaded vanadate cathode.
- The electrode polarization effectively improves with loaded Ni/Fe nanoparticles.
- Composite cathode with Ni/Fe nanocatalyst achieves high current efficiency.
- Direct steam electrolysis is efficient and dominates the process at high voltage.

ARTICLE INFO

Article history:
Received 6 September 2013
Received in revised form
19 November 2013
Accepted 9 December 2013
Available online 17 December 2013

Keywords:
Metal nanoparticles
Steam electrolysis
Vanadate
Solid oxide electrolyser

ABSTRACT

The use of composite electrodes based on $La_{0.7}Sr_{0.3}VO_3$ (LSV) for steam electrolysis has uncovered the tremendous potential and capacity inherent in this material. Unfortunately, this material has a major setback of inefficient electrolysis triggered by limited electrocatalytic activity. In this work, an infiltration method is employed to load catalytic-active metal nanoparticles onto the composite electrodes in order to achieve an activity-enhanced electrode performance. The electrical properties of LSV are methodically explored and correlated to electrode performance. At 800 °C in either pure H_2 or low hydrogen partial pressure (pH_2) of 5%H_2/N_2, the polarization resistance of symmetrical cells with Ni-loaded LSV (LSV-Ni) cathode is largely enhanced, in contrast to bare LSV cathode. Similar improvement is also achieved for the Fe-loaded LSV (LSV-Fe) cathode in a wide range of hydrogen partial pressures of 5%–100%. The Faraday efficiencies of LSV-Ni and LSV-Fe composite cathodes were remarkably improved for electrolysis in either 3%H_2O/4.7H_2/Ar or 3%H_2O/Ar at 800 °C.

1. Introduction

The use of solid oxide electrolyser (SOE), as a high-efficiency electrochemical device for steam electrolysis, has stirred much interest in recent years [1–6] owing to the kinetics and thermodynamics for steam dissociation favoured by high temperature electrolysis. The oxide-ion conducting SOE can directly convert steam into hydrogen with high efficiency at applied potential [7–11].

While nickel-yttria stabilized zirconia (Ni-YSZ) cermets are favoured cathodes for the oxide-ion conducting SOE [3], it requires a large amount of reducing gas to protect Ni from being oxidized. The conversion of Ni to NiO would induce a loss of electrical conductivity and even the failure of the cathodes [12,13]. On the other hand, ceramic cathodes such as $(La_{1-x}Sr_x)(Cr_y, M_{1-y})O_{3-d}$ (M = Mn, Fe, Ti, Co), $La_{1-x}Sr_xTiO_3$ and $Ln_{1-x}Sr_xVO_3$ (Ln = La, Ce) are more redox stable for steam electrolysis whether in a strong or weak reducing atmosphere [14–21]. For instance, ceramic $La_{1-x}Sr_xVO_3$ is recognized as a potentially good anode material for solid oxide fuel cells (SOFC) which could also hold promise for eventual application in solid oxide electrolysers. According to Ge et al. [22,23], $La_{1-x}Sr_xVO_3$ displays high electronic conductivity within the broad temperature range of 500–1000 °C. It also possesses a high potential for sulphur tolerance and significant electrode performance

* Corresponding authors. Department of Energy Materials, School of Materials Science and Engineering, Hefei University of Technology, No. 193 Tunxi Road, Hefei, Anhui 230009, China.
E-mail addresses: xiekui@hfut.edu.cn (K. Xie), ycwu@hfut.edu.cn (Y. Wu).

0378-7753/$ – see front matter © 2013 Elsevier B.V. All rights reserved.
http://dx.doi.org/10.1016/j.jpowsour.2013.12.046

as anode of an oxide-ion conducting SOFC. However, its low catalytic activity towards fuel oxidation restricts its use as SOFC anode.

Three critical tools in the design of materials include infiltration, doped atoms and a proper amount of deficiency [21]. Also important is the preservation of the redox-reversible stable structure with intact optimal conductivity and electrocatalytic properties. The direct electrolysis of CO_2 with $La_{0.75}Sr_{0.25}Cr_{0.5}Mn_{0.5}O_{3-d}$ (LSCM) cathode in an oxide-ion conducting SOE has been newly demonstrated [9]. However, the low current efficiency and large polarization resistance of the ceramic cathode are its major limit. The potential electrical properties of ceramic LSV render it an active anode material for SOFC, with confirmed chemical and electrochemical stability in hydrogen and wet methane [22]. Ceramic LSV is also a potential cathode material for oxide-ion conducting solid oxide electrolysers [23]. LSV can keep a stable structure, maintain high conductivity in a hydrogen atmosphere and exhibit n-type conductivity. This is beneficial for the reducing atmosphere arising from the high concentration of hydrogen produced from the electrolysis. However, this ceramic composite cathode based on LSV-YSZ has insufficient catalytic activity that limits its performance [24].

A catalytically active surface has been reported to be useful to anode performance in SOFC [23–26], with the efficiency of the gas conversion or electrolysis largely enhanced by the catalytic properties of the metal catalyst. Ni, Fe, Pt, and Pd are excellent catalysts for enhancing the performance of the fuel electrodes of solid oxide fuel cells or electrolysers. Nano sized metals can be incorporated into the ceramic via infiltration method, which can significantly reduce the energy for gas conversion and at the same time and enhance the electrical properties of the ceramic. In this study, Ni and Fe nanoparticles were loaded onto the surface of an LSV ceramic substrate in order to improve electrocatalytic activity. The electrochemical performance of the composite electrode was systematically investigated. Steam electrolysis with cathodes based on LSV, LSV-Ni, and LSV-Fe were performed in solid oxide electrolysers with and without the flow of reducing gas over the cathodes.

2. Experimental

All chemicals utilized in this current investigation are of analytical grade unless otherwise specified. All the chemicals in this experiment were purchased from SINOPHARM Chemical Reagent Co., Ltd (China) and used as received without further purification. The LSV were synthesized by a solid-state reaction method in which the powders of La_2O_3, $SrCO_3$ and V_2O_5 were mixed together, ball-milled for 15 min, dried, pressed into pellets and fired at 700 °C for 1 h in air, and was then reduced at 900 °C for 10 h in 5%H_2/Ar to form ceramic LSV [22]. Perovskite $La_{0.8}Sr_{0.2}MnO_{3-d}$ (LSM) powders were synthesized via a combustion method followed by a heat treatment at 1200 °C for 10 h in air [27–30]. The 1-mm thick YSZ electrolyte supports were produced from dry-pressing 8YSZ powders into a ~20 mm − diameter green disk which was subsequently fired at 1500 °C for 10 h [31–35].

To identify the phase formation, X-ray diffraction (XRD) (Cu K_α, D/MAX2500V, Japan) was performed (0.02° min^{-1}). Refinement of the XRD patterns was carried out using GSAS software. A scanning electron microscope (SEM) (JSM–6490LV, JEOL Ltd, Japan) and a field emission scanning electron microscope (FESEM) (SU8020, HITACHI, Japan) were used to characterize the microstructure of electrodes and materials. An energy dispersive spectrometer (EDS) was utilized for determining element distribution. X-ray photoelectron spectroscopy (XPS) (ESCALAB25, Thermo, USA) was performed to determine the chemical state of the elements, before and after, high-temperature reduction. The required amount of LSV powder was pressed into bars and fired in air at 800 °C for 2 h, which were later used for conductivity tests. A multi-meter (Keithley 2000, USA) was used for the conductivity tests which were first performed in air, then in 5%H_2/Ar both at 800 °C for transformation from oxidized LSV (LSV-ox) to reduced LSV (LSV-re), respectively. The oxygen partial pressure was controlled by flowing 5%H_2/Ar and simultaneously recording with an online oxygen sensor (Noveltech Type 1231, Australia).

Slurry was formed with an equal amount by weight of the LSV and YSZ powders in ethyl cellulose–terpineol; the slurry was then printed onto the two opposite surfaces of YSZ discs, to assemble symmetrical cells with the configuration of LSV-YSZ/YSZ/LSV-YSZ. 0.0016 mol mL^{-1} solutions of Ni and Fe were prepared in distilled water from ($Ni(NO_3)_2 \cdot 6H_2O$) and ($Fe(NO_3)_3 \cdot 9H_2O$) respectively. Following which the required amount of nitrates (5 mol%, 10 mol%, 15 mol%, per mol LSV) were infiltrated into the LSV powders which were then heated at 550 °C for 3 h. Thereafter, the prepared slurry was printed onto the surfaces of the YSZ followed by a heat treatment at 1100 °C for 3 h, to form the composite electrodes loaded with NiO or Fe_2O_3 nanoparticles. The Ni mole fractions of 5%, 10% and 15% correspond to mass fractions of 1.4%, 2.9% and 4.7%, respectively. Similarly, the Fe mole fractions of 5%, 10% and 15% equal to the mass fractions of 1.3%, 2.8% and 4.4%, respectively. A silver paste (SS–8060, Xinluyi, China) was used for current collection and printing onto the electrode surface after a heat treatment at 550 °C for 30 min. Silver electrical wires were utilized for external circuits. All the symmetrical cells were tested in a quartz tube, with the two electrodes in the same atmosphere. The AC impedance of the 3 kinds of symmetrical cells were tested as a function of hydrogen partial pressure at a 2-electrode mode and 800 °C using an electrochemical station (IM6, Zahner, Germany) in a frequency range of 1M–0.1 Hz. The hydrogen partial pressure was controlled by mixing different ratios of H_2 and N_2 with the aid of mass flow meters (D08-3F, Sevenstar, China). The symmetrical cells were tested with pure H_2 first and later with pure N_2, which is beneficial to the exsolution of Ni and Fe nanoparticles to load to the LSV-YSZ.

Solid oxide electrolysers with the 3 different kinds of cathodes (LSV-YSZ, Ni-loaded LSV-YSZ and Fe-loaded LSV-YSZ) were prepared as discussed above and then reduced at 800 °C in 5%H_2/Ar, with LSM-YSZ as the anode. The single oxide-ion conducting solid oxide electrolyser was sealed to a home-made testing jig of ceramic paste (JD–767, Jiudian, China) for systematic electrochemical measurements. In the process of steam electrolysis, cathodes (three types) of the solid oxide electrolyser were fed with 3%H_2O/4.7%H_2/Ar and 3%H_2O/Ar with anodes in static air. In the experimental setup, the solid oxide electrolyser was equipped with alumina tubes through which the steam is supplied for electrolysis. The electrochemical tests were performed at a 2-electrode mode. The current–voltage (I–V) curves of the solid oxide electrolysers were tested and obtained. The electrolysis of steam in the solid oxide electrolysers based on LSV, LSV-Ni and LSV-Fe, were performed at different potential loads. The output gas produced from the electrolyzers was analysed with an online gas chromatograph (GC9790II, F.L., China).

3. Results and discussion

3.1. Structure

Fig. 1 shows the XRD Rietveld refinement patterns of LSV reduced at 900 °C for 10 h. The Rietveld refinement was performed with GASA software [36]. The experimental and calculated results for LSV indicated a perovskite structure with space group of Pnma which is consistent with the reported data in a previous work [37]. $LaVO_3$ has been classified to be of the orthorhombic $GdFeO_3$ type

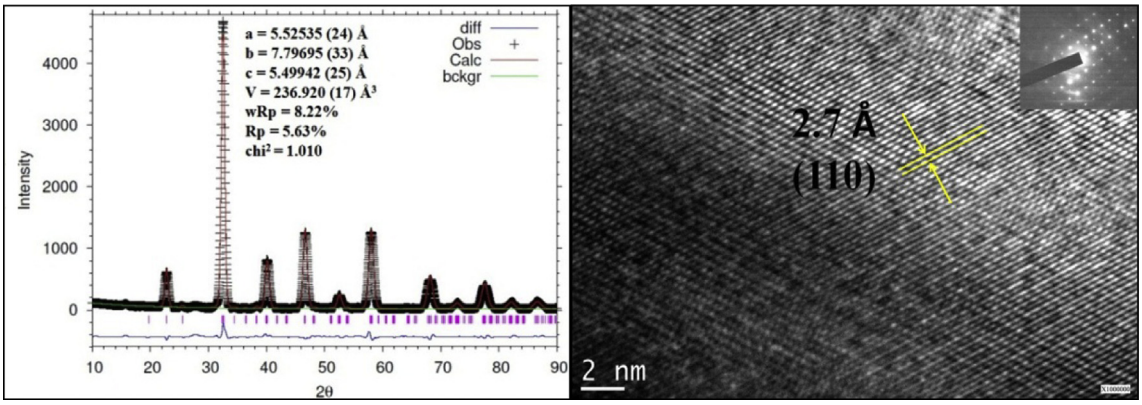

Fig. 1. Rietveld refinement XRD and TEM patterns of LSV powers reduced at 900 °C.

[22]. The Sr element of A-site has influence on the lattice and the structure profiles could fit well into a cubic with increase in Sr content. However, the XRD and TEM results imply that the structures of LSV are more likely to be orthorhombic, nevertheless, the present study suggest it could also fit into a cubic structure. The change in structure is probably due to the chemical state of V element in the perovskite structure. The $V^{4+,5+}$ may co-exist together with V^{3+} even in a reducing atmosphere, which is expected to influence the structure and conductivity and also cause change in the phase structure of reduced $La_{0.7}Sr_{0.30}VO_3$ (LSV-re) between $LaVO_3$ and cubic $(La_{0.50}Sr_{0.50})VO_{2.95}$ (PDF no. 33-1343).

3.2. Conductivity

In order to study the change in electrical properties of the LSV in a reducing atmosphere from oxidized state to reduced state, conductivity tests were carried out both in air and with the oxygen partial pressure (Po_2) fixed at 10^{-19} in 5%H_2/Ar at 800 °C. Fig. 2(a) shows that the conductivity of oxidized LSV improves with temperature, demonstrating a typical p-type semiconducting behaviour. The LSV-ox is not a single phase. Rather, it is composed of the monoclinic $LaVO_4$ and triclinic $Sr_2V_2O_7$ dissolved in each other. As shown in Fig. 2(a), the mixed conductivity of the oxidized LSV is as low as 10^{-3} to 10^{-4} S cm^{-1} because the oxidized sample is typical semiconductor with the charge carrier of hole [22]. However, the high reducing activity of the oxidized LSV was observed as shown in Fig. 2(b). The conductivity of the sample significantly shifts from a semiconductor to an electronic conductor even after a short-term reduction at 800 °C for 40 min. This indicates that the reduction of V element and the formation of LSV-re can be attributed to the improvement and shifts in the electrical conductivity.

3.3. XPS

To describe the different chemical states of the elements in the samples, core level spectroscopy of V_{2p}, La_{3d}, Sr_{3d} and O_{1s} for the oxidized and reduced LSV were obtained using XPS as shown in Figs. 3 and 4. The XPS data were fitted using a Shirley-type background subtraction method, and the background functions for different spectra of the elements were fitted by 80% Gaussian and 20% Lorenz. Fig. 3(a1) and (a2) show the V_{2p} core-level XPS results of oxidized and reduced LSV samples, in which the spin-orbit splitting shows a double of $2p_{1/2}$ and $2p_{3/2}$ excitation. The V^{5+} ($2p_{1/2}$) peak was observed at 524.68 eV, whereas V^{5+} ($2p_{3/2}$) showed a peak at 517.29 eV as reflected in Table 1 [38]. For the reduced LSV, V^{4+} ($2p_{3/2}$) has close binding energy with V^{3+} ($2p_{3/2}$) peak at ~516.07 eV, which makes it difficult to distinguish. Based on the XPS data, V^{5+} is the main chemical state for LSV-ox while the ratio of $V^{3+,4+}/V^{5+}$is ~73.9:26.1 for LSV-re. In contrast, the V^{3+} is the main chemical state for reduced LSV samples as shown in Fig. 3(a2). The V element in B site has a positive effect on the conductivity of perovskite structure in a reducing atmosphere. While it has been reported that LSV-ox was not a single phase [22], the LSV-re was able to form a single phase structure with high conductivity when most of the V^{5+} is reduced to$V^{3+,\ 4+}$ (Table 2).

The core-level XPS spectra of O_{1s}, La_{3d}, and Sr_{3d} are presented in Figs. 3 and 4. The O^{2-}_{1s} peak was observed at 530.40 eV for oxidized samples and 530.33 eV for reduced samples. The peaks of La^{3+} $3d_{3/2}$ and $3d_{5/2}$ were observed at 851.70 eV and 834.89 eV for oxidized samples, and 851.83 eV and 835.04 eV for reduced samples, respectively [39,40]. For oxidized samples, Sr $3d_{3/2}$ appeared at 135.27 eV and $3d_{5/2}$ at 133.61 eV, 135.10 eV and 133.40 eV for reduced samples, respectively [41]. As shown in Figs. 3 and 4, the

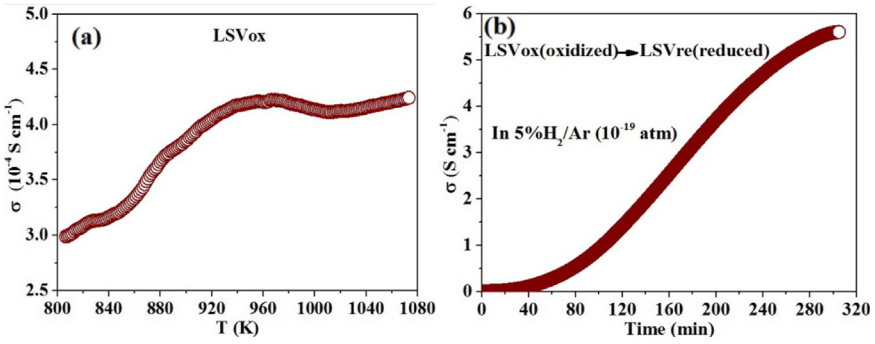

Fig. 2. Total conductivity of LSV-ox in air and LSV-re in 5%H_2/Ar with oxygen partial pressure of 10^{-19} at 800 °C.

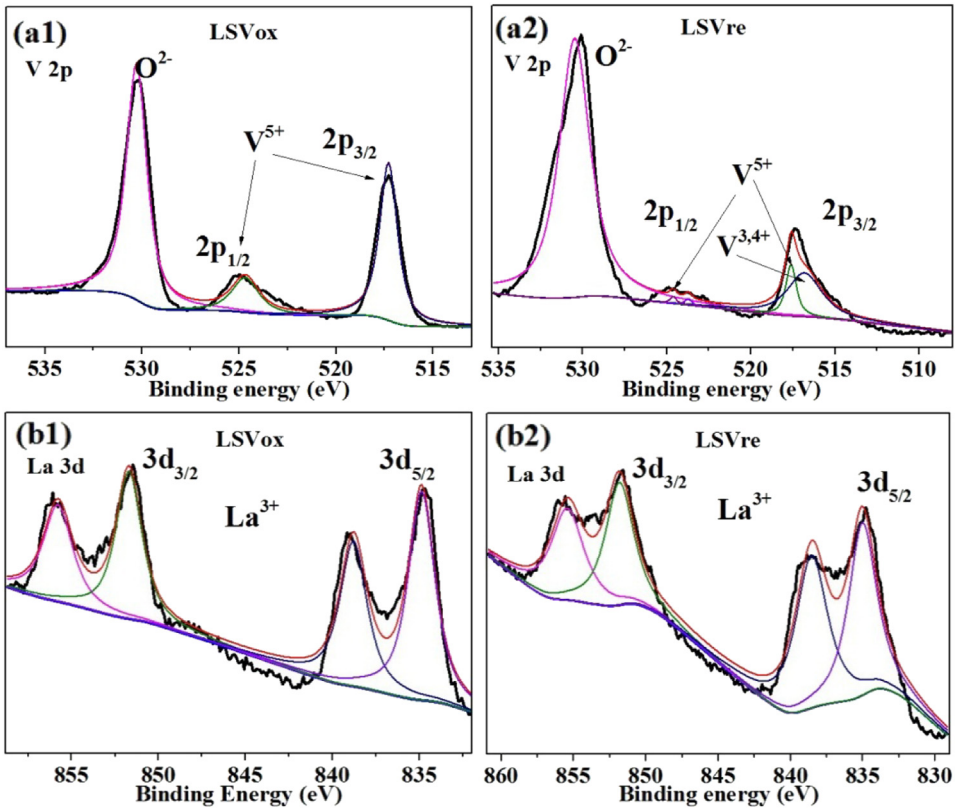

Fig. 3. V_{2p}, La_{3d} X-ray photoelectron spectroscopy of oxidized and reduced LSV.

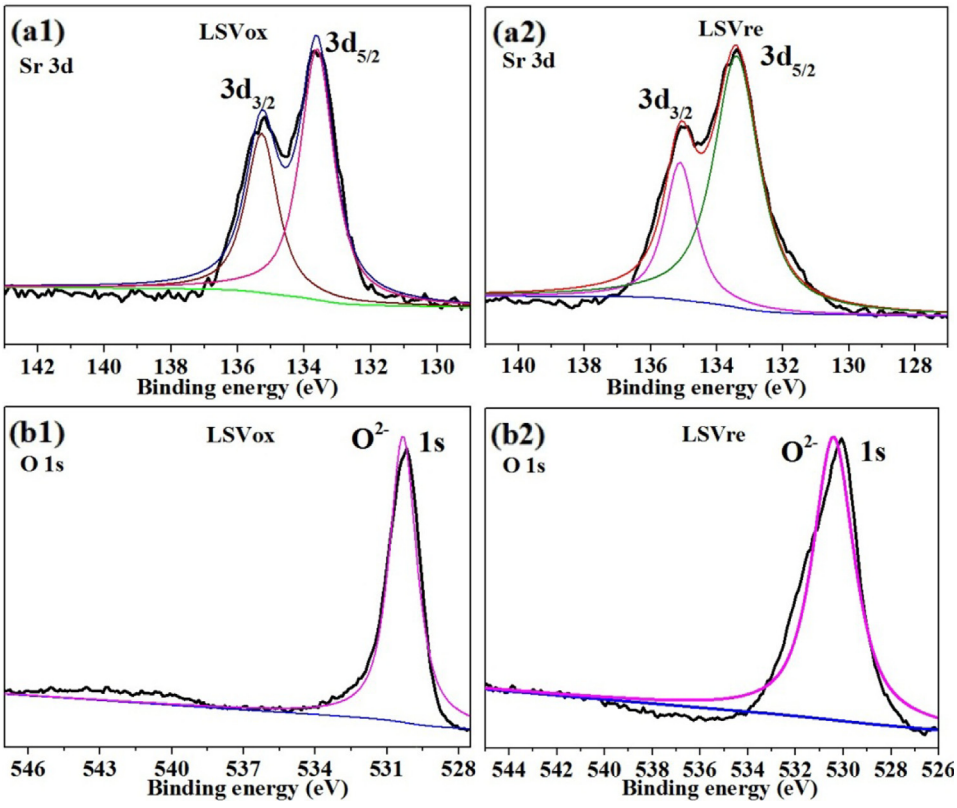

Fig. 4. Sr_{3d}, O_{1s} X-ray photoelectron spectroscopy of oxidized and reduced LSV.

Table 1
The binding energy for the different elements of LSV-ox and LSV-re.

Element		Binding energy (eV)				
		LSV-ox			LSV-re	
		$2p_{1/2}$	$2p_{3/2}$		$2p_{1/2}$	$2p_{3/2}$
V	V^{5+}	524.68	517.29	V^{5+}	524.69	517.29
	V^{3+}		516.07	$V^{3+,4+}$		516.07
		$3d_{3/2}$	$3d_{5/2}$		$3d_{3/2}$	$3d_{5/2}$
La	La^{3+}	851.70	834.89	La^{3+}	851.83	835.04
Sr	Sr^{2+}	135.27	133.61	Sr^{2+}	135.10	133.40
		1s			1s	
O	O^{2-}	530.40		O^{2-}	530.33	

chemical state of La, Sr, and O was stable for oxidized and reduced samples. The slight change of chemical state of the elements between oxidized and reduced samples may be due to the structural changes accompanies the conversion of oxidized LSV to reduced LSV.

3.4. Symmetrical cells

Fig. 5 corresponds to the AC impedance studies of symmetrical cells with electrodes based on LSV, Ni-loaded LSV and Fe-loaded LSV after reduction in 5%H_2/Ar, versus hydrogen partial pressure at 800 °C. The series resistance (R_s) and the polarization resistance (R_p), depicted by the first intercept and the difference between the first and second intercepts, were calculated by Zview software as reported in our previous work [5]. Increase in the hydrogen partial pressure lowered the R_p of the symmetrical cells while R_s remained stable over a wide range of hydrogen partial pressure. The R_s of the symmetrical cell based on LSV (~3.21 Ω cm^2) was comparable to those of cells based on LSV-Ni and LSV-Fe. The comparable R_s values suggest that the infiltration of Ni or Fe does not have a significant effect on the R_s of the cells. The R_p of the symmetrical cell based on LSV (8.32 Ω cm^2) at low hydrogen partial pressure of 5% dropped significantly to 1.65 Ω cm^2 and 3.05 Ω cm^2 for Ni-loaded LSV and Fe-loaded LSV, respectively. In such a reducing atmosphere, the enhanced electrocatalytic activity of the cells that led to improved polarization resistance may be attributed to the Ni or Fe nanoparticles. The improved charge transfer in TPB caused by the Ni or Fe nanoparticles in the electrodes may have led to the reduction in polarization resistance. Since catalytic activity is enhanced in a stronger reducing atmosphere, increasing the hydrogen partial pressure also improved the R_p of symmetrical cells based on LSV. In pure hydrogen atmosphere, the R_p of the Ni-loaded LSV (~0.73 Ω cm^2) was relatively lower than the R_p of the symmetrical cell based on LSV (~1.27 Ω cm^2). In the case of the Fe-loaded LSV, a low R_p of ~3 Ω cm^2 at low hydrogen partial pressure was further favourably lowered to 1.91 Ω cm^2 in pure hydrogen. It appears that increasing the hydrogen partial pressure to create a stronger reducing atmosphere was able to reduce and activate the electrodes, enhance electrocatalytic activity and thus reduce the electrode polarization resistances.

Table 2
The R_s and R_p of the symmetrical cells based on LSV, LSV-Ni and LSV-Fe at different hydrogen partial pressures at 800 °C.

	pH_2 (%)	5	60	80	100
LSV	R_s (Ω cm^2)	3.21	3.26	3.24	3.25
	R_p (Ω cm^2)	8.32	1.28	1.27	1.27
LSV-Ni	R_s (Ω cm^2)	3.20	3.19	3.19	3.19
	R_p (Ω cm^2)	1.65	0.84	0.76	0.73
LSV-Fe	R_s (Ω cm^2)	3.15	3.13	3.13	3.13
	R_p (Ω cm^2)	3.05	2.79	2.50	1.91

3.5. Steam electrolysis

Fig. 6 presents the microstructures of the solid oxide electrolysers with the configuration of (cathode) LSV-YSZ/YSZ/LSM-YSZ (anode). The silver current collection layer is ~7 μm thick. Both porous cathode and anode layers are ~12 μm in thickness, which adhere well to the 1-mm thick YSZ electrolyte. Fig. 7 shows the current–voltage curves of the solid oxide electrolysers with cathodes based on LSV, LSV-Ni and LSV-Fe pre-reduced in 5%H_2/Ar, then tested in 3%H_2O/4.7%H_2/Ar and 3%H_2O/Ar at 800 °C. As can be seen from the I–V curves for the 3%H_2O/4.7%H_2/Ar, the open circuit voltages (OCVs) of solid oxide electrolysers reached approximately 0.92 V, 0.98 V, and 0.95 V for the LSV, LSV-Ni and LSV-Fe cathodes. This is probably because the I–V test process is not at equilibrium. From 0 V to the OCV, the electrochemical cell is indeed a solid oxide fuel cell in 3%H_2O/4.7%H_2/Ar. Based on the current density, less than 4% H_2 was consumed, which suggests that it has little influence on the stability of the electrodes. The I–V curves of the solid oxide electrolyser are far from linear, with a slope change of approximately 1.1 V. Above 1.1 V, the current densities of the LSV electrodes with catalytic particles increased steeply compared to the bare LSV electrode. The onset of steam electrolysis to produce hydrogen can be anticipated at about 1.1 V. The I–V curves showed that the current densities for LSV, LSV-Ni and LSV-Fe in 3%H_2O/4.7% H_2/Ar stabilized above 1.8 V, but decreased for LSV-Ni in 3%H_2O/Ar at an applied voltage of ~1.9 V. The less positive voltages must have led to large polarization resistances. This indicates that there must have been an increase in the kinetics of the steam reduction, which consequently resulted in the local starvation process at high voltages. At this point, one is tempted to suggest the conversion of steam to hydrogen may limit the total steam electrolysis at high current density.

In order to study the anticipated change in R_s and R_p, in-situ AC impedance tests were performed to characterize the solid oxide electrolysers with LSV-YSZ, LSV-Fe-YSZ and LSV-Ni-YSZ cathodes exposed in either 3%H_2O/4.7%H_2/Ar or 3%H_2O/Ar. It was observed that, in both 3%H_2O/4.7%H_2/Ar and 3%H_2O/Ar, R_s values were stabilized at approximately 4 Ω cm^2, whereas R_p values decreased considerably as applied voltage increased from 0 to 2.0 V. It is assumed that increasing the voltage activated the electrodes to the extent that R_p decreased remarkably. Increasing the voltage is expected to improve electrode polarization, following the improved kinetic process of the electrode. Two semicircles were noted on the impedance spectra: the high-frequency arcs (R_1) and low-frequency arcs (R_2). At high frequency, R_1 of the solid oxide electrolysers with cathodes based on bare LSV, LSV-Ni and LSV-Fe was stable in 3%H_2O/4.7H_2/Ar. With Ni and Fe nanoparticles incorporated into the cathodes, R_1 improved in 3%H_2O/Ar. This suggests that the metal nanoparticles were able to improve the performance of the cathodes, in agreement with results of the symmetrical cells tests as shown in Fig. 5. The R_1 from the charge transfer at cathodes/YSZ interfaces was generally stable. Since charge transfer is the main limitation at low voltages, R_1 at high voltages may partly contribute to the electrochemical process of the cathodes. At low frequency, it was observed that mass transfer dominated the process of the solid oxide electrolysers. This may be due to the gas conversion, dissociative adsorption and species transfer at TPB. Fig. 8 shows that the two arcs exist together in the range of 0–2.0 V at the applied potentials. This is an indication that the charge transfer of the cathodes/electrolyte interfaces still exists at high voltages. However, gas diffusion becomes the dominant limitation as the voltage increases. The charge transfer limit ceases to be the main limitation as steam electrolysis takes over as the dominant process at high voltages.

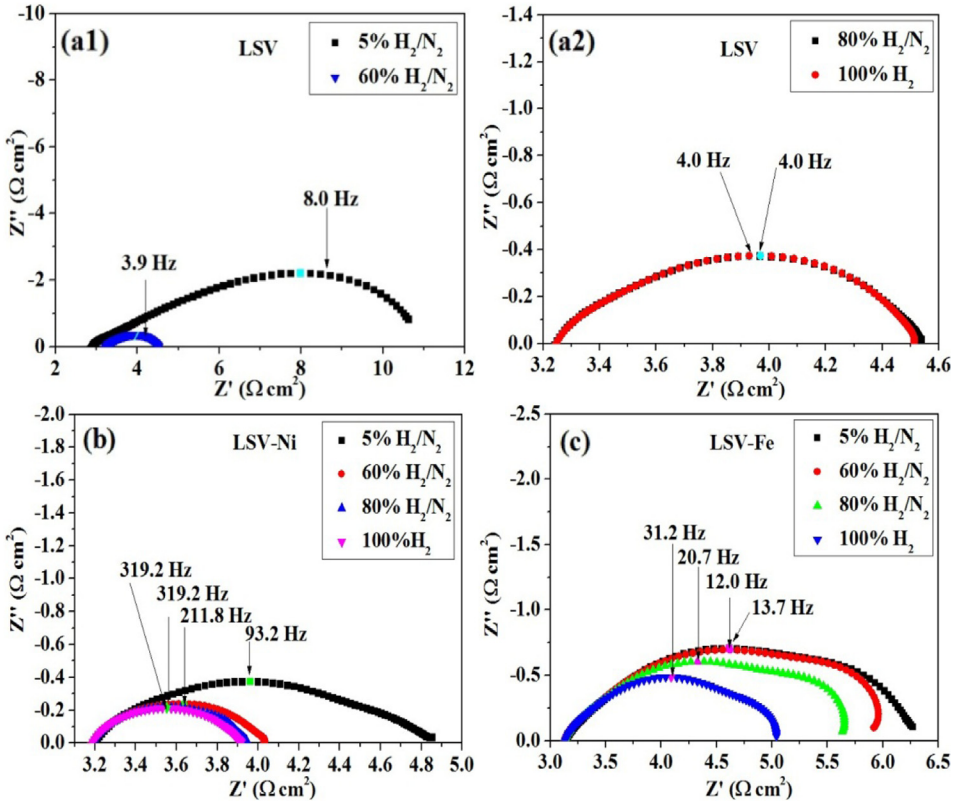

Fig. 5. AC impedance spectroscopy of YSZ-supported symmetrical cells based on LSV, LSV-Ni and LSV-Fe electrodes at different hydrogen partial pressure at 800 °C.

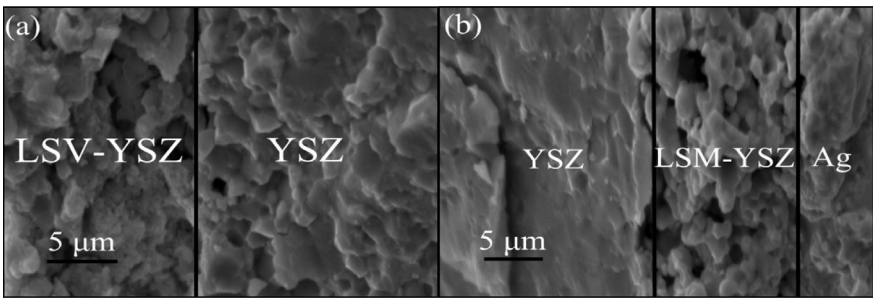

Fig. 6. Cross sectional SEM micrographs for solid oxide electrolyzers of (a) LSV-YSZ/YSZ and (b) YSZ/LSM-YSZ/Ag.

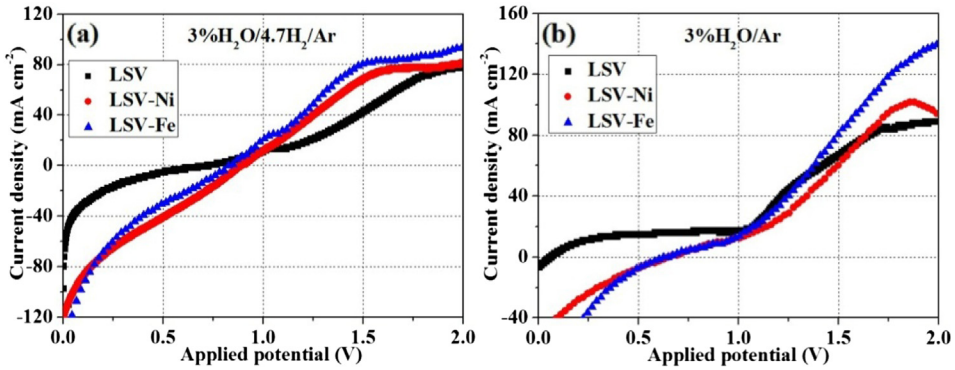

Fig. 7. Current–voltage curves of the solid oxide electrolyzers with cathodes based on LSV, LSV-Ni and LSV-Fe fed with (a) 3%H_2O/4.7%H_2/Ar and (b) 3%H_2O/Ar at 800 °C, respectively.

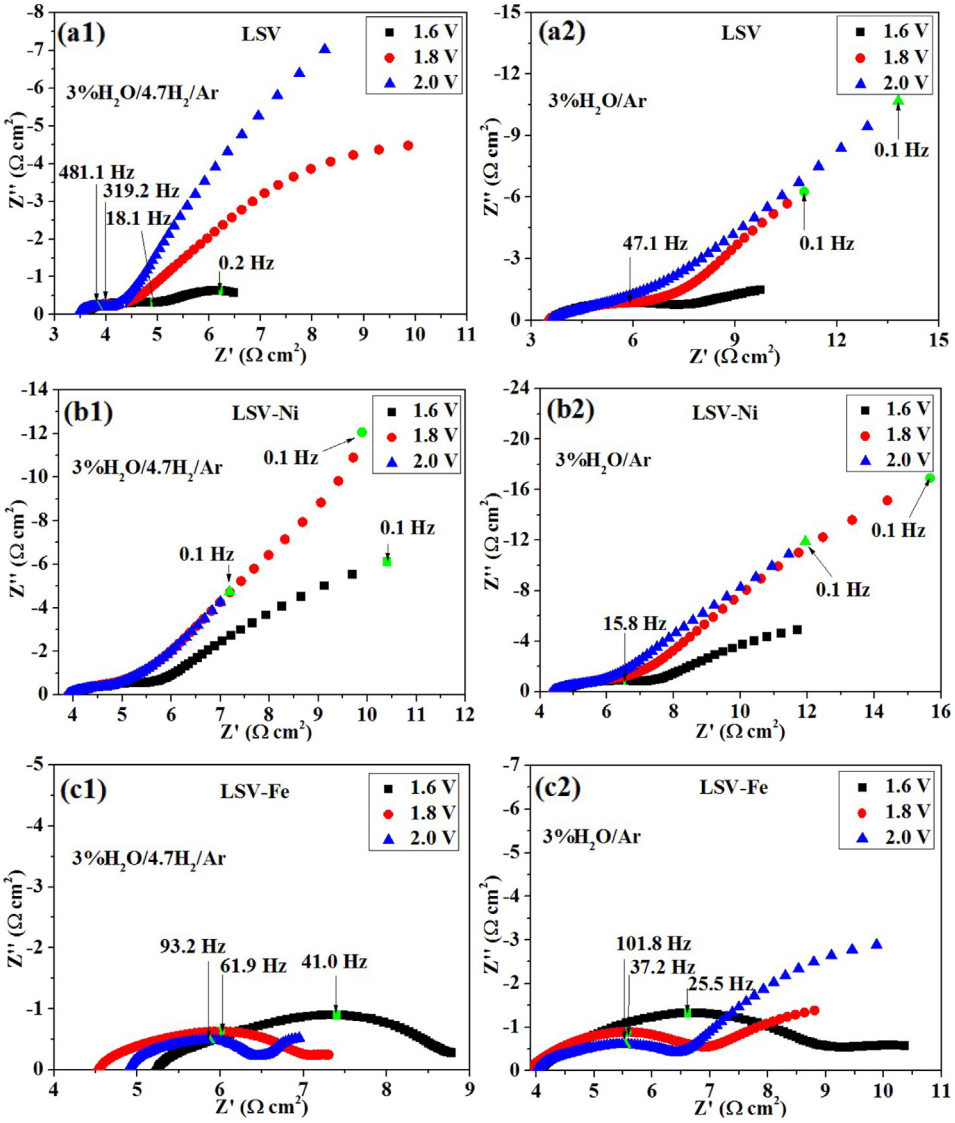

Fig. 8. In-situ AC impedance spectroscopies of solid oxide electrolyzers with cathodes based on LSV, LSV-Ni and LSV-Fe fed with 3%H_2O/4.7%H_2/Ar and 3%H_2O/Ar at 800 °C, respectively.

Fig. 9 depicts hydrogen production by steam electrolysis at 800 °C using solid oxide electrolysers based on LSV, LSV-Ni and LSV-Fe cathodes fed with 3%H_2O/4.7%H_2/Ar. At the applied potential of 1.6 V, the production of hydrogen was ~0.20 ml min^{-1} for LSV, compared to the improved hydrogen production of ~0.46 ml min^{-1} and ~0.43 ml min^{-1} for LSV-Ni and LSV-Fe, respectively. This further confirms that the loading of Ni and Fe was able to improve electrical properties and significantly increase the production of hydrogen with an accompanied increased electrocatalytic activity. Thus, the loading of Ni and Fe nanoparticles improved electrode performance for the production of hydrogen, by increasing the active TPB. For LSV-Ni, it was observed that the current density dropped when the voltage was above 1.5 V as shown in Fig. 7. This may be due to the limitation of the steam conversion process, owing to the local starvation of steam. In total, the Faraday efficiencies with the Ni- and Fe-loaded LSV cathodes in 3%H_2O/4.7%H_2/Ar at all potentials were enhanced by approximately 20%, relative to the bare LSV. Again, this establishes that the nanoparticles were able to improve the steam electrolysis process.

The performance of the solid oxide electrolysers based on LSV, LSV-Ni and LSV-Fe composite cathodes in the absence of hydrogen was also investigated. The results are shown in Fig. 10. At the applied potential of 1.6 V, current density increased for the LSV cathodes loaded with Fe and Ni nanoparticles. The Faraday efficiency moderately increased when applied potential was increased from 1.3 to 2.0 V. Higher potentials produce stronger reducing conditions in the cathode and further activate the electrode for the electrochemical reduction of steam. However, the current efficiency was further enhanced by ~10% at 1.6 V owing to the enhanced performance of the cathodes loaded with Ni and Fe nanoparticles. It was observed that cathodes with LSV-Fe produced the highest current density, suggesting that the Fe catalyst has better electrocatalytic activity for the direct steam electrolysis in the absence of hydrogen protection. Fig. 11 presents the SEM and XRD patterns of the cathodes based on LSV-Ni and LSV-Fe after the short-term test for the steam electrolysis. The cathodes show a porous structure which is beneficial to gas diffusion, adsorption and desorption. It was observed that there exist typical diffraction peaks corresponding to Ni ($2\theta = 44.5°$) and Fe nanoparticles ($2\theta = 44.6°$) as

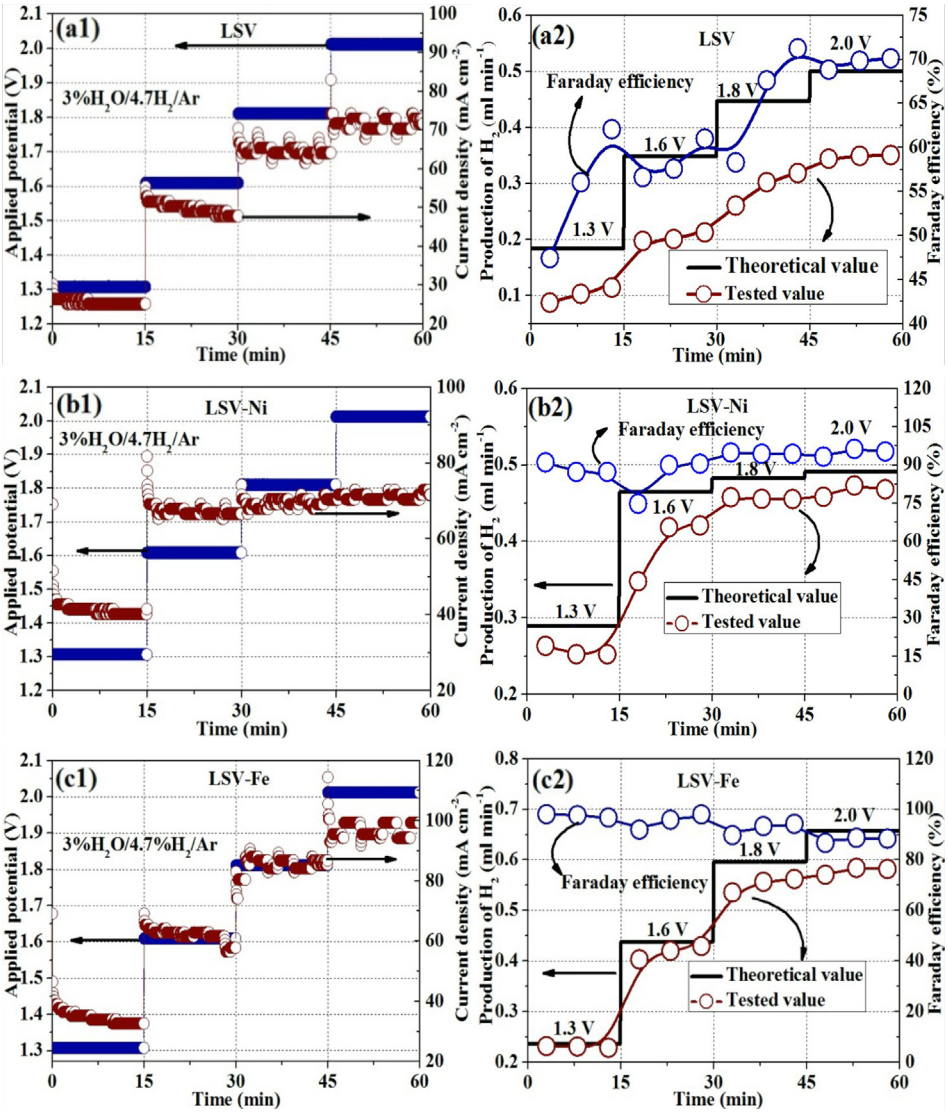

Fig. 9. Electrolysis performance of the solid oxide electrolyzers with cathodes based on LSV, LSV-Ni and LSV-Fe at different applied potentials of 1.3 V, 1.6 V, 1.8 V and 2.0 V in 3% H_2O/4.7%H_2/Ar at 800 °C.

shown in Fig. 11. The peaks suggest the presence of Ni and Fe in the metal state during the process of steam electrolysis. In addition, no phase change was seen for the LSV electrode substrate after exposure to either 3%H_2O/4.7%H_2/Ar or 3%H_2O/Ar in the process of steam electrolysis. This implies that the LSV electrode may be stable as the cathode in an electrolysis mode. Further investigation on the chemical stability and catalytic activity of the LSV cathode for high temperature steam electrolysis is on-going.

Fig. 12 displays the performance of the cathodes loaded with different contents of Ni or Fe in the solid oxide electrolysers fed in 3%H_2O/4.7%H_2/Ar at 800 °C. The current density shows good stability at the applied potentials of either 1.3 or 1.6 V. The current density for cathodes loaded with 10 mol% Ni was significantly higher than that loaded with 5 mol% Ni in the solid oxide electrolysers. However, the current density and hydrogen production improved a little when 15 mol% Ni was loaded to the cathode. Based on this, the optimum metal loading is approximately 10%. FESEM images and EDS maps presented in Figs. 13 and 14 confirm that the nano-sized metal particles were uniformly distributed in the cathodes, except for the cathodes loaded with 15 mol% Fe which showed agglomeration of Fe metal in Fig. 14 (d). The extended TPB in the porous cathodes benefits the electrocatalytic process of the steam electrolysis. Fig. 14 indicates slight agglomeration of Ni metal, which may lead to performance degradation and/or the composite cathodes limitation.

4. Conclusions

In this work, Ni- and Fe-loaded LSV composite cathodes were successfully prepared and utilized for steam electrolysis. The loading of Ni or Fe nanoparticles significantly improved the electrocatalytic activity of the composite electrodes and enhanced the electrode polarization resistance of the symmetrical cells as well as the solid oxide electrolysers. Accordingly, the current densities were enhanced largely for the solid oxide electrolysers with LSV-Ni and LSV-Fe cathodes for steam electrolysis in 3%H_2O/4.7%H_2/Ar. The current efficiencies were improved by approximately 20% in a wide range of applied potentials. In summary, this study demonstrates the synergistic effects of catalytic-active Ni or Fe nanoparticles with

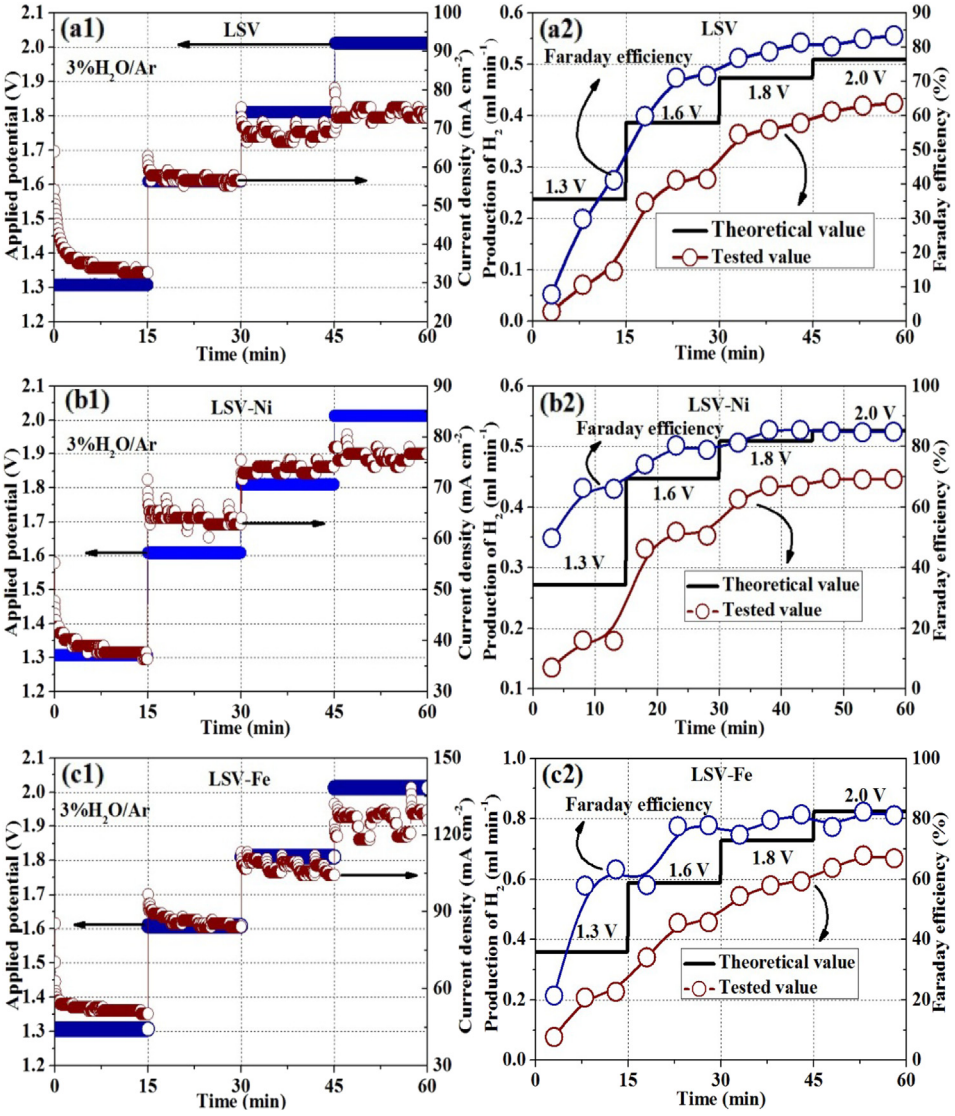

Fig. 10. Electrolysis performance of the solid oxide electrolyzers with cathodes based on LSV, LSV-Ni and LSV-Fe at different applied potentials of 1.3 V, 1.6 V, 1.8 V and 2.0 V in 3% H_2O/Ar at 800 °C.

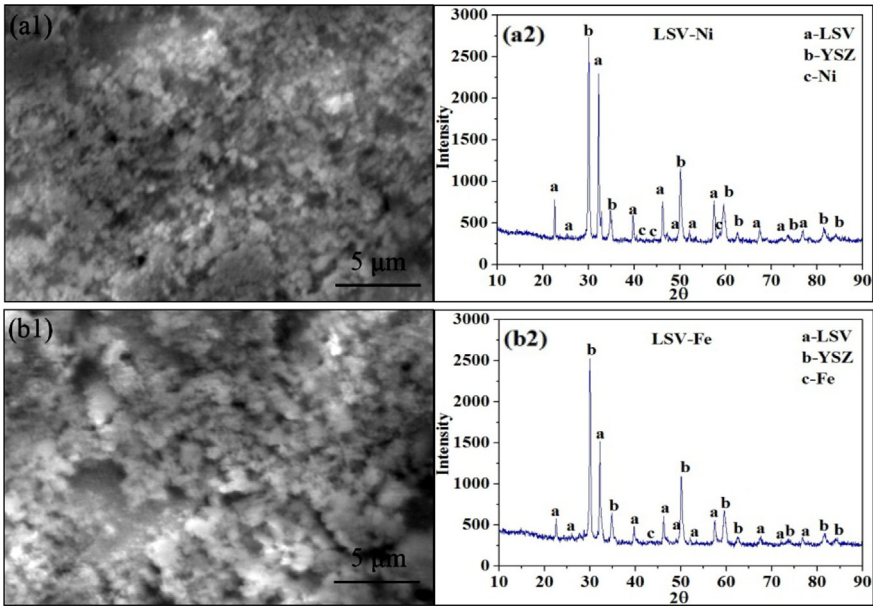

Fig. 11. SEM images and XRD patterns of the cathodes based on Ni loaded LSV-YSZ and Fe loaded LSV-YSZ after short-term test of 7 h.

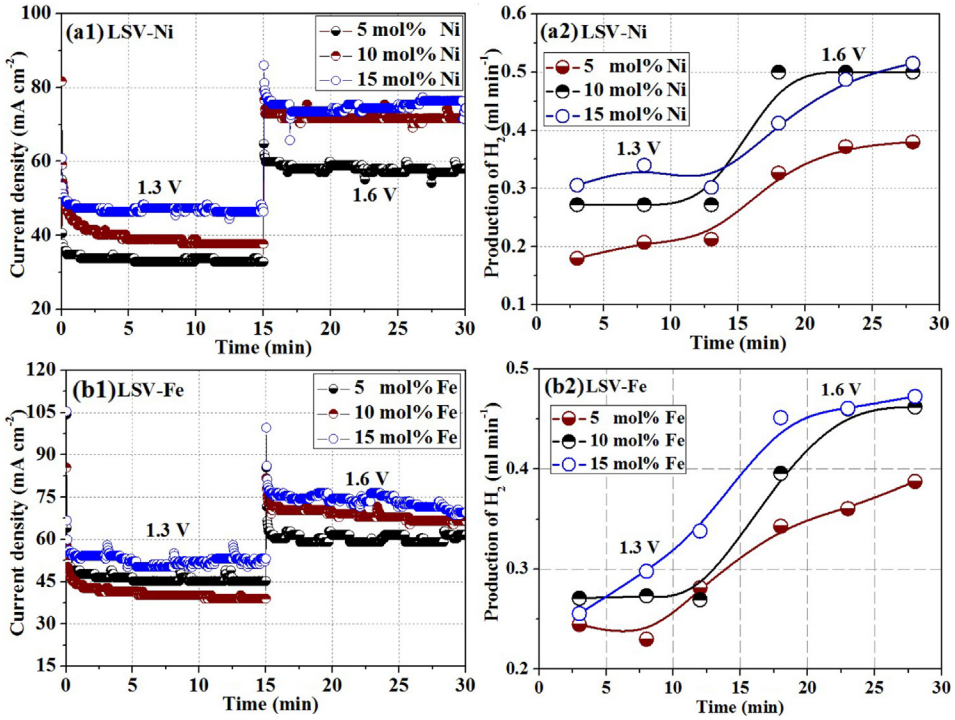

Fig. 12. Electrolytic performance of the SOE with cathodes based on LSV loaded with different amounts of Ni and Fe at applied potentials of 1.3 V and 1.6 V in 3%H_2O/4.7%H_2/Ar at 800 °C.

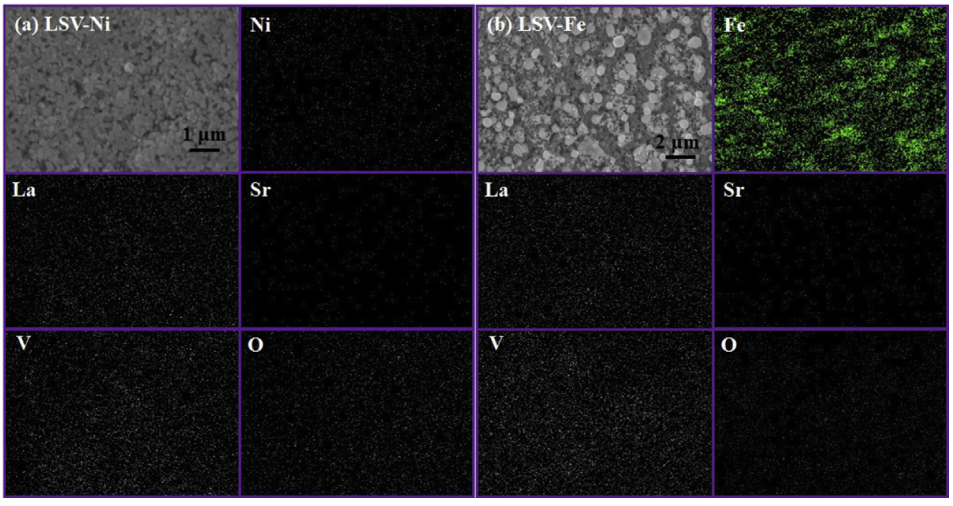

Fig. 13. FESEM images and EDS maps of the cathodes based on LSV with 10 mol% Ni or Fe reduced at 800 °C.

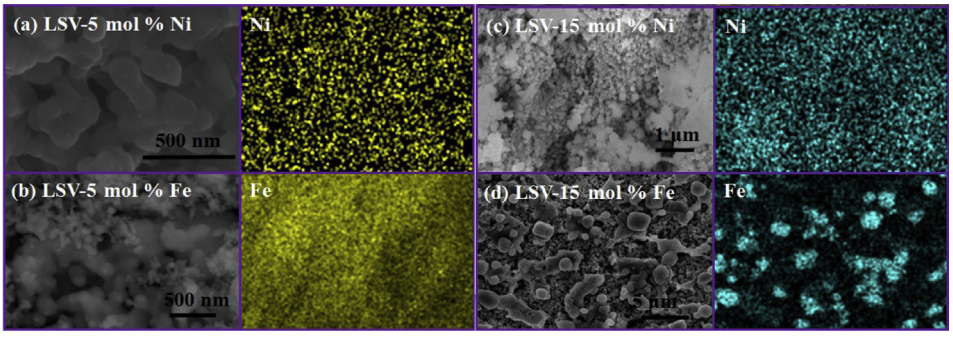

Fig. 14. FESEM images and EDS maps of the cathodes based on LSV with different contents of reduced Ni and Fe at 800 °C.

a ceramic LSV substrate, leading to their improved performance in high-temperature steam electrolysis.

Acknowledgement

This work is supported by the Natural Science Foundation of China No. 21303037, China Postdoctoral Science Foundation No. 2013M53150 and the Fundamental Research Funds for the Central Universities No. 2012HGZY0001.

Appendix A. Supplementary data

Supplementary data related to this article can be found at http://dx.doi.org/10.1016/j.jpowsour.2013.12.046.

References

[1] J. Karczewski, B. Bochentyn, S. Molin, M. Gazda, P. Jasinski, B. Kusz, Solid State Ionics 221 (2012) 11–14.
[2] K. Xie, Y.Q. Zhang, G.Y. Meng, J.T.S. Irvine, J. Mater. Chem. 21 (2011) 195–198.
[3] Y.X. Li, J.E. Zhou, D.H. Dong, Y. Wang, J.Z. Jiang, H.F. Xiang, K. Xie, Phys. Chem. Chem. Phys. 14 (2012) 15547–15553.
[4] S.S. Li, Q.Q. Qin, K. Xie, Y. Wang, Y.C. Wu, J. Mater. Chem. A 1 (2013) 8984–8993.
[5] Y. Gan, J. Zhang, Y.X. Li, S.S. Li, K. Xie, J.T.S. Irvine, J. Electrochem. Soc. 159 (2012) F1–F5.
[6] S.S. Li, K. Xie, J. Electrochem. Soc. 160 (2013) F224–F233.
[7] K. Xie, Y.Q. Zhang, G.Y. Meng, J.T.S. Irvine, Energy Environ. Sci. 4 (2011) 2218–2222.
[8] S.H. Jensen, X.F. Sun, S.D. Ebbesen, R. Knibbe, M. Mogensen, Int. J. Hydrogen Energy 35 (2010) 9544–9549.
[9] S.S. Xu, S.S. Li, W.T. Yao, D.H. Dong, K. Xie, J. Power Sources 230 (2013) 115–121.
[10] J.E. O'Brien, M.G. McKellar, C.M. Stoots, J.S. Herring, G.L. Hawkes, Int. J. Hydrogen Energy 34 (2009) 4216–4226.
[11] X.D. Yang, J.T.S. Irvine, J. Mater. Chem. 18 (2008) 2349–2354.
[12] M.H. Pihlatie, H.L. Frandsen, A. Kaiser, M. Mogensen, J. Power Sources 195 (2010) 2677–2690.
[13] M.H.D. Othman, N. Droushiotis, Z.T. Wu, G. Kelsall, K. Li, Adv. Mater. 23 (2011) 2480–2483.
[14] V.B. Vert, F.V. Melo, L. Navarrete, J.M. Serra, Appl. Catal. B Environ. 115–116 (2012) 346–356.
[15] N. Danilovic, A. Vincent, J.L. Luo, K.T. Chuang, R. Hui, A.R. Sanger, Chem. Mater. 22 (2010) 957–965.
[16] A.D. Aljaberi, J.T.S. Irvine, J. Mater. Chem. A 1 (2013) 5868–5874.
[17] J.S. Park, J. Luo, L. Adijanto, J.M. Vohs, R.J. Gorte, J. Power Sources 222 (2013) 123–128.
[18] S.M. Plint, P.A. Connor, S.W. Tao, J.T.S. Irvine, Solid State Ionics 177 (2006) 2005–2008.
[19] C. Peng, B.W. Wang, A. Vincent, J. Mater. Sci. 47 (2012) 227–233.
[20] J.C. Ruiz-Morales, J. Canales-Vázquez, C. Savaniu, D. Marrero-López, W.Z. Zhou, J.T.S. Irvine, Nature 439 (2006) 568–571.
[21] E.Y. Konysheva, X.X. Xu, J.T.S. Irvine, Adv. Mater. 24 (2012) 528–532.
[22] X.M. Ge, S.H. Chan, J. Electrochem. Soc. 156 (2009) B386–B391.
[23] X.M. Ge, L. Zhang, Y.N. Fang, J. Zeng, S.H. Chan, RSC Adv. 1 (2011) 715–724.
[24] J.S. Park, I.D. Hasson, M.D. Gross, C. Chen, J.M. Vohs, R.J. Gorte, J. Power Sources 196 (2011) 7488–7494.
[25] X.M. Ge, C.J. Fu, S.H. Chan, Phys. Chem. Chem. Phys. 13 (2011) 15134–15142.
[26] X.M. Ge, C.J. Fu, S.H. Chan, Electrochim. Acta 56 (2011) 5947–5953.
[27] J. Mizusakia, Y. Yonemura, H. Kamata, K. Ohyama, N. Mori, H. Takai, H. Tagawa, M. Dokiya, K. Naraya, T. Sasamoto, H. Inaba, T. Hashimoto, Solid State Ionics 132 (2000) 167–180.
[28] Y. Sakaki, Y. Takeda, A. Kato, N. Imanishi, O. Yamamoto, M. Hattori, M. Iio, Y. Esaki, Solid State Ionics 118 (1999) 187–194.
[29] K.F. Chen, N. Ai, S.P. Jiang, Int. J. Hydrogen Energy 37 (2012) 10517–10525.
[30] Y. Zheng, R. Ran, Z.P. Shao, J. Phys. Chem. C 112 (2008) 18690–18700.
[31] S.S. Li, Y.X. Li, Y. Gan, K. Xie, G.Y. Meng, J. Power Sources 218 (2012) 244–249.
[32] J.J. Choi, J.H. Choi, J. Ryu, B.D. Hahn, J.W. Kim, C.W. Ahn, W.H. Yoon, D.S. Park, J. Eur. Ceram. Soc. 32 (2012) 3249–3254.
[33] Y.H. Gong, W.J. Ji, B. Xie, H.Q. Wang, Solid State Ionics 192 (2011) 505–509.
[34] S. Cho, Y.N. Kim, J.H. Kim, A. Manthiram, H.Y. Wang, Electrochim. Acta 56 (2011) 5472–5477.
[35] Q.S. Zhu, B.A. Fan, Solid State Ionics 176 (2005) 889–894.
[36] A.C. Larson, R.B. Von Dreele, General Structure Analysis System (GSAS), Los Alamos National Laboratory Report, LAUR, 2004, pp. 86–748.
[37] P. Bordet, C. Chaillout, M. Marezio, Q. Huang, A. Santoro, S.W. Cheong, H. Takagi, C.S. Oglesby, B. Batlogg, J. Solid State Chem. 106 (1993) 253–270.
[38] G.C. Bond, S. Flamerz, Appl. Catal. 46 (1989) 89–102.
[39] J. Kasperkiewicz, J.A. Kovacich, D. Lichtman, J. Electron Spectrosc. Relat. Phenom. 32 (1983) 123–132.
[40] Y. Uwamino, T. Ishizuka, H. Yamatera, J. Electron Spectrosc. Relat. Phenom. 34 (1984) 67–78.
[41] R.P. Vasquez, Surf. Sci. Spectra 1 (1992) 24–30.